Article

Influences of Cr and Co on the Growth of Thermally Grown Oxide in Thermal Barrier Coating during High-Temperature Exposure

Weifang Zhang, Jingyu Zhang, Hongxun Wang * [ID]**, Weitao Lou and Xiaopeng Liu** [ID]

School of Reliability and Systems Engineering, Beihang University, Haidian District, Beijing 100191, China; zhangweifang@buaa.edu.cn (W.Z.); jingyuzhang@buaa.edu.cn (J.Z.); louweitao@buaa.edu.cn (W.L.); liuxiaopeng@buaa.edu.cn (X.L.)

* Correspondence: wanghongxun@buaa.edu.cn; Tel.: +86-10-8231-5759

Abstract: Thermal barrier coating (TBC) is a critical material in the aerospace domain to increase the lifetime of gas turbine components subjected to thermal load. The properties of TBC are strongly related to the growth of thermally grown oxide (TGO) whose main constituent is Al_2O_3. However, the oxidation of Cr and Co can affect the growth of TGO, which is not studied sufficiently. In this paper, high-temperature exposure at 1000 °C was performed to investigate the effect of Cr and Co oxides on TGO growth. The morphology and composition analysis of the interface between the ceramic top coat and the bond coat (TC/BC) were investigated by using scanning electron microscopy (SEM) and the energy dispersion spectrum (EDS). The thermodynamics and kinetics of oxidation were analyzed. The results indicated that the oxidation kinetics basically followed the sub-parabolic law with exposure time. Additionally, the major factor affecting the formation of oxides was the diffusion rate at the initial stage of exposure, then oxides depended on thermodynamics, and the oxidation was influenced by both of them in the last stage. The major elements to be oxidized were different at different stages. Moreover, the replacement reaction of Cr_2O_3 and the phase conversion of Al_2O_3 resulted in thickness variations of the TGO and Al-depleted zone during high-temperature exposure.

Keywords: thermal barrier coating (TBC); high-temperature exposure; thermally grown oxide (TGO); Cr oxide; oxidation kinetics

1. Introduction

Thermal barrier coating (TBC) is one of the most widely used multilayer coating systems of gas turbines in aerospace, energy and other fields to improve the efficiency and prolong the lifetime of components by reducing their temperature and enhancing oxidation resistance [1]. TBC is usually composed of the ceramic (yttria partially stabilized zirconia (YSZ)) top coat and MCrAlY (M is Co, Ni or both) bond coat. These coatings are applied by electron beam physical vapor deposition (EB-PVD) or plasma spray (PS) technology [2,3]. The bond coat plays an important role in the TBC system, which improves the physical compatibility between the ceramic top coat and the substrate, and thus the ceramic top coat can combine closely with the substrate. Moreover, elements in the bond coat diffuse to the ceramic top coat and the bond coat (TC/BC) interface to react with oxygen, and the thermally grown oxide (TGO), which is the mixture of Al, Cr and Co oxides, is formed during high-temperature exposure. The continuous and dense oxide scale can enhance the high temperature oxidation resistance and hot corrosion resistance of components. Failure of the coating is related to the critical thickness of Al_2O_3 scale at the TC/BC interface; thus the main factor affecting the durability of a coating is recognized as the oxidation rate of the bond coat [4]. The failure of TBC is related to the conversion

from initial α-Al_2O_3 to α-Cr_2O_3 and (CoNi)(CrAl) spinel [5]. The thermal stress caused by a thermal expansion coefficient mismatch between the spinel oxides and Al_2O_3 results in the formation of a crack at the interface of TC/TGO/BC [6]. The oxidation resistance of TBC is determined by the dense Al_2O_3 with a slow growth rate, thus TBC with high Cr and Al contents can prevent itself from corrosion and oxidation [7]. However, Cr and Co in the bond coat can also react with oxygen, and detrimental oxides like $Co(Al,Cr)_2O_4$ spinel are formed when severe Al depletion happens. Therefore, the continuous and dense oxide scale cannot be formed to protect the substrate, which can accelerate the failure of TBC [6]. The formation of Cr and Co oxides is determined by the diffusion rate of Cr and Co as well as the growth rate of Al_2O_3. The oxidation behaviors of Cr and Co have an influence on the oxidation process of Al, in turn. Furthermore, the oxidation resistance of TBC is gradually reduced because of the consumption of Al and Cr in the bond coat [8]. Most research related to the oxidation resistance of TBC focuses mainly on the growth behaviors of Al_2O_3 [9–11]. It is reported by Keyvani [10] that non-protective oxides are formed rapidly at the initial oxidation stage and the growth of TGO is under the diffusion control; and the effects of diffusion rate on the oxidation of Cr and Co in the Ni alloy are studied in detail by Allen [12]. The failure of a TBC system depends on the TGO growth behaviors during the oxidation process [11]. TGO growth causes volume variation at the TC/BC interface, which results in out-of-plane stress at the interface. The crack propagates in the TBC system through the opening and growth in the ceramic and the limited crack nucleation and propagation related to TGO [13,14]. However, there are a few investigations that pay attention to the effects of Cr and Co oxides on the TGO growth behavior. Therefore, it is of great significance to investigate the oxidation behaviors of Cr and Co in order to improve oxidation resistance and prolong the lifetime of TBC. Most research mainly pays attention to the temperature range of TBC from 1000 to 1200 °C by using EB-PVD technology. When the temperature is larger than 1170 °C, the volume expansion of phase conversion can result in the TBC cracking. Also, the YSZ agglomerates with the rise in temperature, and thus the failure of TBC can occur more easily at relatively high temperature [15,16]. This paper focuses on the investigation of the influence of Al, Cr and Co oxides on TGO growth behavior, and the failure of the TBC system is not expected to occur during the high-temperature exposure. Therefore, the test temperature needs to be set below 1170 °C. In this paper, the effects of oxidation behaviors of Cr and Co on TGO growth behavior at the TC/BC interface during high-temperature exposure at 1000 °C were studied. The paper is organized as follows. Firstly, the material and experimental design are introduced. Secondly, the kinetics of the high-temperature exposure are analyzed, respectively. Thirdly, the morphology and composition analysis of the oxide scales at the TC/BC interface are investigated. Finally, the oxidation thermodynamics are studied, and the conclusions are given.

2. Material and Experiments

In this study, a cast Ni-based superalloy K444 specimen with size of 2.8 mm $\times$ Ø16.0 mm was used as the substrate. Firstly, the specimen was polished with 800-grit emery papers prior to TBC deposition. Then, a CoCrAlY bond coat was deposited on the K444 superalloy substrate using the EB-PVD technique, and the thickness of the CoCrAlY bond coat was 150 μm. After that, the bond-coated specimen was annealed for 4 h at 1000 °C in a vacuum to acquire a homogeneous microstructure, and then its surface was strengthened by shot-peening [17]. Finally, the YSZ top coat of thickness 60 μm was deposited on the bond-coated specimen by EB-PVD. The YSZ top coat is composed of (8% $\pm$ 1%) Y_2O_3 and ZrO_2. The profile of the TBC specimen is shown in Figure 1. The chemical composition of the substrate and CoCrAlY bond coat are given in Tables 1 and 2, respectively.
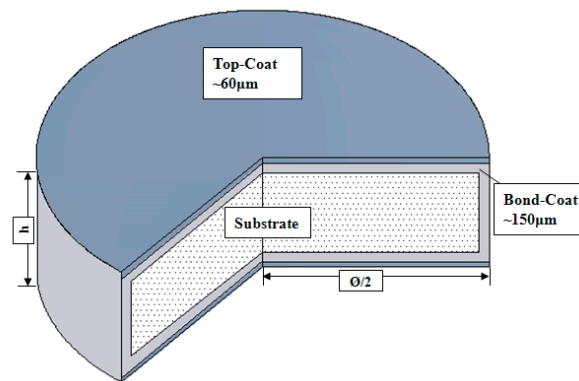
Figure 1. The profile of the thermal barrier coating (TBC) specimen.

Table 1. Chemical composition of K444.

Element	Ni	C	Cr	Co	W	Mo	Al	Ti	Nb	Hf
Content (wt.%)	Bal.	0.085	15.28	10.48	5.13	2.08	3.10	4.40	0.19	0.31

Table 2. Chemical composition of CoCrAlY.

Element	Co	Cr	Al	Ni	Y	Hf	Zr	Si	Fe	C
Content (wt.%)	61.83	23.12	12.25	1.24	0.67	0.15	0.23	0.27	0.21	0.03

A high-temperature exposure experiment at 1000 °C was carried out in air using the chamber electric furnace (SIOM, Shanghai, China) with an accuracy of 5 °C. Under each experimental condition, three parallel specimens were set. The specimens were hung by nickel chrome wire, then put into crucibles. When the furnace temperature rose to 1000 °C at the rate of 20 °C·min^{-1}, the crucibles with specimens were quickly put into the furnace and separated by a suitable distance in order to ensure the same oxidation environment. The high-temperature exposure was begun when the furnace temperature recovered to 1000 °C. During the high-temperature exposure, the furnace was ventilated by opening the furnace door for 5 s per 2 h to ensure enough oxygen. Specimens 1–3 were oxidized for 10, 50, 80, 120, 160 and 200 h, which were weighed by using an analytical balance (FA1004N, JINGHUA Instruments, Shanghai, China) with an accuracy of 0.1 mg to analyze the oxidation kinetics. Specimens 4–7 were oxidized for 10, 50, 120 and 200 h, respectively. The parallel specimens at each exposure time were also weighed by using an analytical balance. The morphology and composition analysis of the TC/BC interface were investigated by using scanning electron microscopy (SEM, SUPPER 55, Carl Zeiss AG, Oberkochen, Germany) equipped with an energy dispersion spectrum (EDS, QUANTAX-200, Bruker Corporation, Billerica, MA, USA). The phase analysis was carried out by the X-ray diffraction technique (XRD, X'Pert PRO, PANalytical B.V., Almelo, The Netherlands). The thickness changes of the TGO and Al-depleted zone were measured manually, respectively. Finally, the oxidation thermodynamics of the high-temperature exposure test were investigated.

3. Results

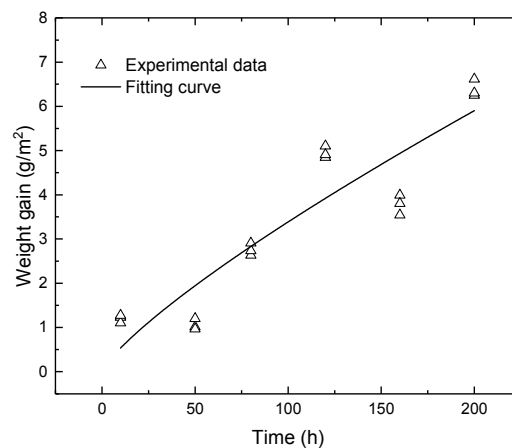### 3.1. The Analysis of Oxidation Kinetics

To analyze the oxidation mechanism during the high-temperature exposure, the oxidation rate determined by the oxidation kinetics needs to be considered. The weight gains of three parallel specimens were measured at 10, 50, 80, 120, 160 and 200 h, respectively. Moreover, the successive differential method was used to calculate the average oxidation rate. The weight gains and average oxidation rates of TBC at each exposure time are summarized in Table 3.

Table 3. The weight gains and average oxidation rates of TBC at each exposure time at 1000 °C.

Oxidation Time (h)	Weight Gain (g·m^{-2})			Average Oxidation Rate (g·m^{-2}·h^{-1})
	Specimen 1	Specimen 2	Specimen 3	
10	1.2292	1.1043	1.2767	0.1203
50	1.0133	0.9642	1.2015	0.0212
80	2.6356	2.7359	2.9102	0.0345
120	4.8482	5.1049	4.9084	0.0413
160	3.5454	3.9941	3.8053	0.0236
200	6.2510	6.6165	6.3044	0.0320

The oxidation kinetics of TGO can be expressed by Equation (1), where y is the weight gain of oxide scale (g·m^{-2}), t is the time (h), k_p represents the rate constant, and n is the exponent. After fitting experimental data of the weight gain in Table 3, the oxidation kinetics of TBC during the high-temperature exposure at 1000 °C is presented in Figure 2. In the presented case, n is 1.248 and k_p is 0.046 as obtained from Figure 2, and thus the weight gain increased with time follows the sub-parabolic law. The TBC shows a fast weight gain at the initial stage of exposure, and the corresponding average oxidation rate is 0.1203 g·m^{-2}·h^{-1}; then a relatively slower weight gain can be seen at the later stages of exposure whose average oxidation rate is lower than 0.05 g·m^{-2}·h^{-1}, and thus the oxidation rate gradually slows down at the later stage of exposure.

$$y^n = k_p t \qquad (1)$$

Figure 2. The oxidation kinetics of TBC during the high-temperature exposure at 1000 °C.

3.2. Morphology and Composition Analysis of Oxide Scales

The morphologies of specimens were characterized by using SEM to observe the TBC surface deposited by EB-PVD, as shown in Figure 3. It can be seen that the microstructure of the YSZ top coat was columnar crystal whose growth direction was perpendicular to the substrate surface [18]. In order to study the phase composition of the bond coat, the specimen was polished by emery paper until the YSZ top coat was completely removed and the remaining thickness of the bond coat was about 100 µm. The XRD pattern of the bond coat is shown in Figure 4a. It can be seen that the bond coat consisted of γ-Co and β-CoAl phases. Figure 4b is the morphology of the cross-section of the bond coat. The bond coat was composed of a bright zone and a dark zone. After the EDS analysis, the chemical compositions of the bright Zone A and the dark Zone B are listed in Table 4. The Al content in the dark Zone B was larger than that in the bright Zone A. After comparing with the XRD pattern of the bond coat, it could be seen that the bright Zone A was γ-Co solid phase, and the dark Zone B was β-CoAl phase. As the β-CoAl phase was rich in Al, Al was mainly supplied by the β-CoAl

phase during the high-temperature exposure. With the diffusion of Al in the bond coat to the TC/BC interface, a large amount of β-CoAl phase was consumed. The β-CoAl phase was depleted and only γ-Co was left near the TGO/BC interface, thus the Al-depleted zone occurred.
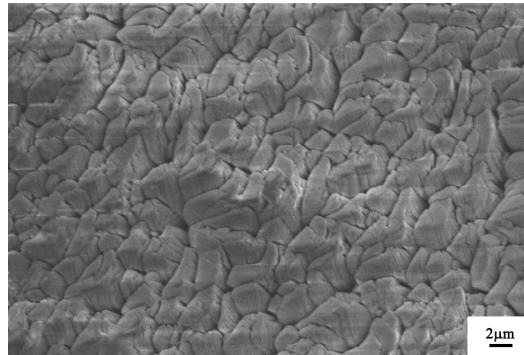

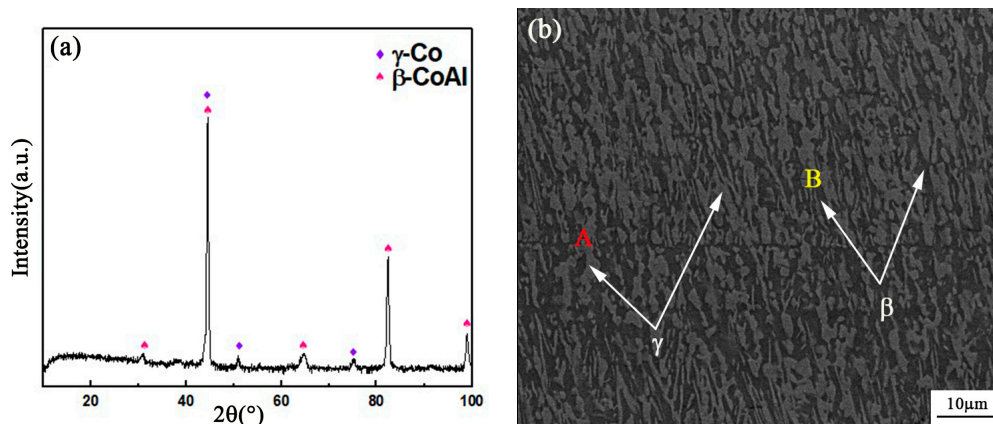**Figure 3.** The micrographs of TBC surface deposited by electron beam physical vapor deposition (EB-PVD).

Figure 4. The phase analysis and morphology of the bond coat: (**a**) the X-ray diffraction (XRD) pattern of the bond coat; (**b**) the morphology of the bond coat.

Table 4. Chemical compositions of the bright Zone A and dark Zone B in Figure 4b.

Zone	Content	Co	Cr	Al	Ni	Y
A	wt.%	71.82	24.84	3.21	0.09	0.03
	at.%	67.05	26.29	6.55	0.09	0.02
B	wt.%	70.30	21.17	8.17	0.34	0.03
	at.%	62.49	21.33	15.86	0.31	0.02

The morphology of the TBC surface after 200 h of exposure is shown in Figure 5. The surface of the TBC basically remained flat, but some partial zones cracked and had blisters and fragments, such as in the red box. The high magnification view of the red box in Figure 5a is shown in Figure 5b. Along the crack propagation path, there was the square pyramid crystal whose morphology was different from the surrounding columnar crystal as shown in Point A. At Point A, Cr and Co oxides formed during the high-temperature exposure after detection by EDS. The chemical composition of oxide at Point A is summarized in Table 5.
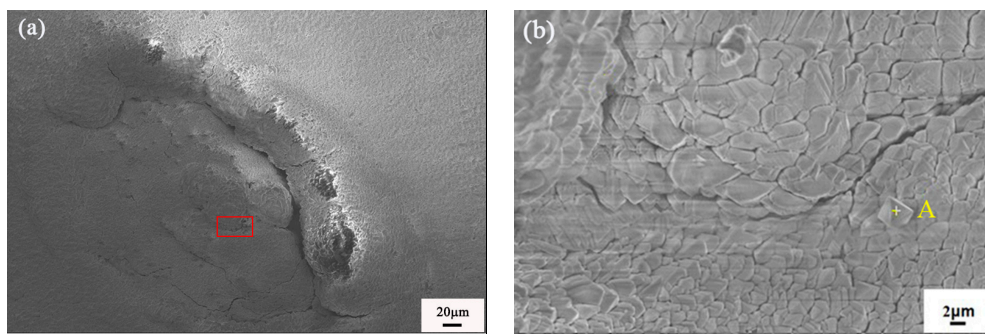
Figure 5. The micrographs of the TBC surface after 200 h of exposure: (**a**) the morphology of blisters and fragments; (**b**) high magnification view of the red box in (**a**).

Table 5. Chemical composition of Point A in Figure 5.

Content	O	Co	Cr	Al	Y
wt.%	55.97	30.55	10.13	3.23	0.12
at.%	83.11	11.85	4.14	0.57	0.33

The morphologies of the TC/BC interface oxidized for 10, 50, 120 and 200 h at 1000 °C were observed by using SEM to investigate the growth behavior of TGO, respectively. The EDS line-scan was analyzed at different exposure times along the straight line which was perpendicular to the TC/BC interface, and the content changes of oxide scale along the straight line of the TC/BC interface were as below. additionally, the thickness variations of the TGO and Al-depleted zone during the high-temperature exposure was measured repeatedly along the lines which were parallel to the growth direction of the TGO and Al-depleted zone, and the experimental data were averaged. The morphology and composition analysis of the TC/BC interface before the high-temperature exposure and after 10 h of exposure are shown in Figures 6 and 7, respectively. The morphology of the TC/BC interface exposed for 10 h did not change significantly compared with that before the high-temperature exposure, and the thickness of the TGO increased a little. The thickness of the TGO exposed for 10 h was 0.57 μm, which was larger than that before the high-temperature exposure whose thickness was 0.41 μm. The change of oxygen content was very low, thus a small amount of oxides were formed after 10 h of exposure. The EDS analysis shows that the contents of Al, Cr and Co increased, and the contents of Cr and Co showed a sharp peak before the Al content at the TC/BC interface. Therefore, Cr and Co were oxidized before Al at the initial stage. This result was also demonstrated by Keyvani [10].
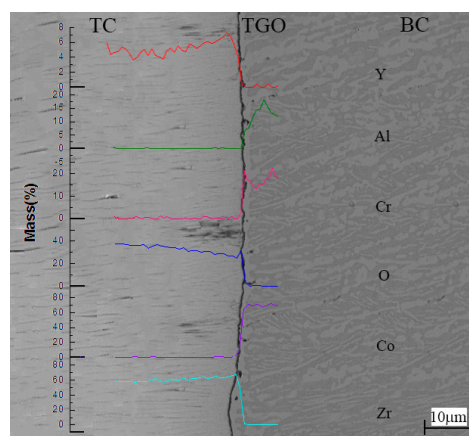

Figure 6. The morphology and composition analysis of the top coat and bond coat (TC/BC) interface before the high-temperature exposure.
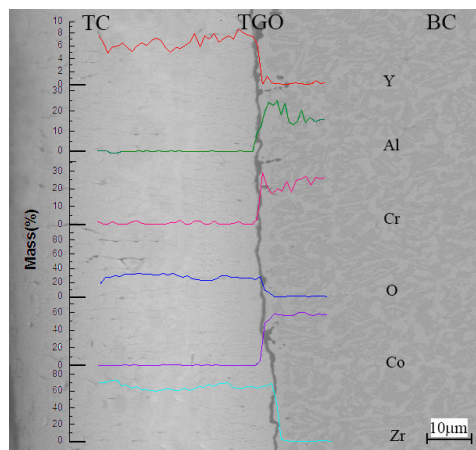
Figure 7. The morphology and composition analysis of the TC/BC interface after 10 h of exposure.

Figure 8 shows the morphology and composition analysis of the TC/BC interface after high-temperature exposure for 50 h. The TGO thickness was 1.40 μm, which increased significantly compared with the thickness after 10 h of exposure, and there were oxides to be oxidized at this stage. Moreover, the Al-depleted zone occurred near the TGO/BC interface due to the consumption of Al, and the thickness of the Al-depleted zone was 3.49 μm, which indicated that the β-CoAl phase was depleted near the TGO/BC interface and a large quantity of Al_2O_3 was formed. As Al showed a peak before Cr and Co, this indicates that Al was preferentially oxidized. Additionally, the contents of Al and Cr increased compared with those after 10 h of exposure, and thus the oxides formed at this stage were mainly Al_2O_3 and a small amount of Cr oxide.
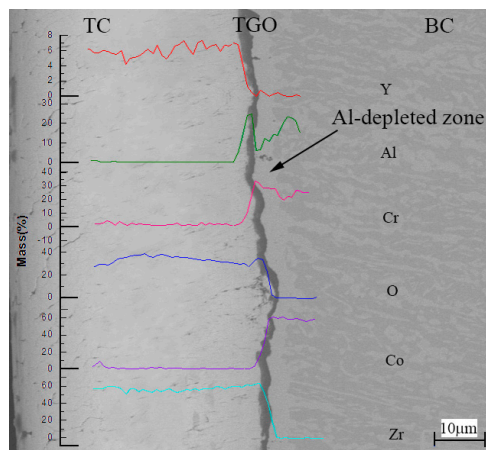

Figure 8. The morphology and composition analysis of the TC/BC interface after 50 h of exposure.

Figure 9 shows the morphology and composition analysis of the TC/BC interface after high-temperature exposure for 120 h. The TGO thickness changed from 1.40 μm exposed for 50 h to 2.47 μm exposed for 120 h, and the thickness of Al-depleted zone increased from 3.49 to 5.69 μm. A large quantity of Al at the TGO/BC interface was consumed, the β-CoAl phase was decreased, which further led to the Al-depleted zone thickening. A large amount of Al_2O_3 was formed, and thus a dense and continuous oxide scale was basically formed at this stage. With the declination of the Al content, there was no sufficient Al to be oxidized to form Al_2O_3 at the TGO/BC interface, Cr and Co began to be oxidized, and thus the Cr and Co oxides had an impact on the formation of Al_2O_3 [19]. It was observed that the Co content increased notably, which indicated that a small amount of Co was oxidized at this stage.
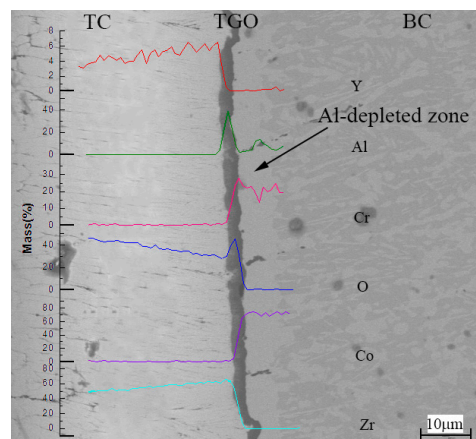
Figure 9. The morphology and composition analysis of the TC/BC interface after 120 h of exposure.

The morphology and composition analysis of the TC/BC interface after 200 h of exposure is shown in Figure 10. The TGO thickness decreased from 2.47 µm exposed for 120 h to 1.80 µm exposed for 200 h, and the thickness of the Al-depleted zone declined from 5.69 to 4 µm. From the EDS analysis, Cr and Co content increased after 200 h of exposure, and thus Cr and Co oxides were formed at this stage. With Al diffused out of the deep layer of the bond coat to the TGO/BC interface during the high-temperature exposure from 120 to 200 h, the Al content at the TGO/BC interface gradually increased in 200 h. Therefore, the thickness of the Al-depleted zone decreased. When the Al content met the requirement for the formation of Al_2O_3, Al started to be oxidized again. Oxygen preferentially reacted with Al, which indicated that the Al content had an influence on the formation of Cr and Co oxides. More Cr and Co oxides were formed at this stage.
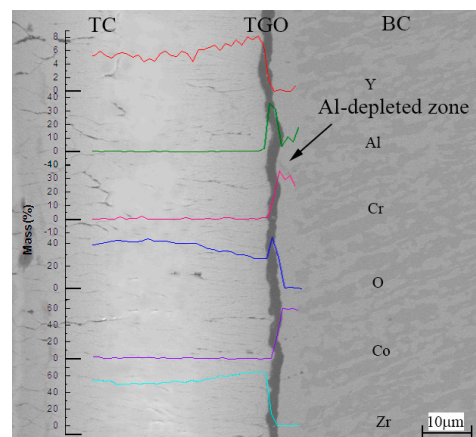

Figure 10. The morphology and composition analysis of the TC/BC interface after 200 h of exposure.

In order to investigate intuitively the composition analysis of Al, Cr and Co oxidized for 10, 50, 120 and 200 h at 1000 °C, the content changes of Al, Cr and Co in the TGO are shown in Figure 11. It can be seen that the contents of Al, Cr and Co increased after 10 h of exposure, and thus Al_2O_3 and Cr and Co oxides were formed at this stage. After exposure for 50 h, Al, Cr and Co contents all increased, and as the Al content increased notably, the major oxides was Al_2O_3. The Al-depleted zone occurred at this stage with the consumption of Al. Therefore, the oxidation rate of Al_2O_3 after 120 h of exposure was smaller than that after 50 h of exposure. This indicated that the oxides formed after 120 h of exposure was a large quantity of Al_2O_3 and a small amount of Co. But the Cr content declined, which indicates that Cr was nearly not oxidized at this stage. During the exposure from 120 to 200 h, it can be seen that the Al content decreased but Cr and Co contents increased. When the Al content

was not sufficient to be oxidized, Cr and Co started to be oxidized, thus a small amount of Cr and Co oxides were formed, which indicated that the Cr and Co oxides affected the formation of Al_2O_3.
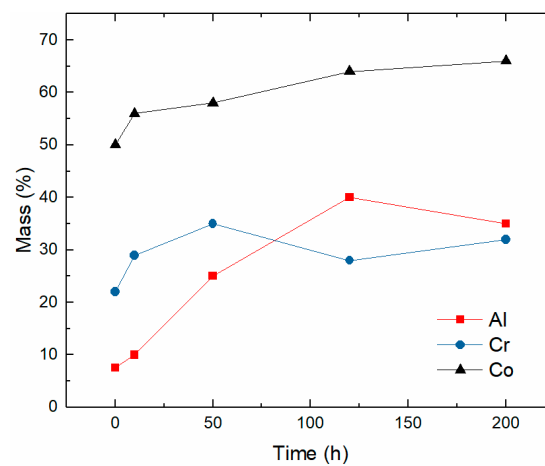

Figure 11. The content changes of Al, Cr and Co in the thermally grown oxide (TGO) during the high-temperature exposure.

The elemental maps of the TGO were investigated by using EDS after high-temperature exposure for 200 h. Figure 12 is a SEM image of the cross-section and corresponding EDS elemental maps. It can be seen that the dark area of TGO contained Cr, Co, Al and O elements at the TC/BC interface. The Cr and Co oxides were surrounded by Al_2O_3 near the TGO/BC interface, which indicated that the oxides were mainly Al_2O_3 and a small amount of Cr and Co oxides. The chemical composition of the red box in Figure 12 is shown in Table 6. The EDS analysis shows that the red box of TGO was mainly composed of Al_2O_3, which did not contain Cr and Co oxides. Therefore, TGO was mainly composed of Al_2O_3 near the TC/TGO interface, and a small amount of Cr and Co oxides at the TGO/BC interface after the high-temperature exposure for 200 h.
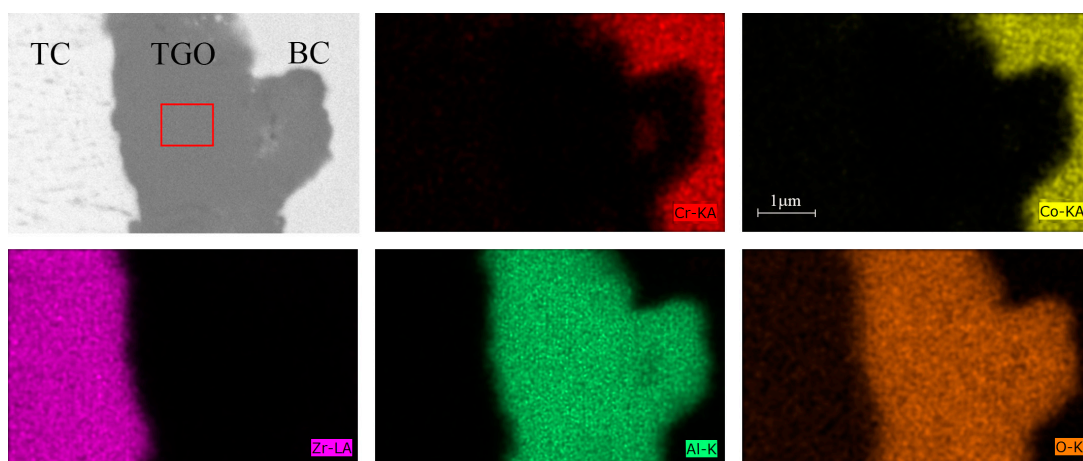

Figure 12. A scanning electron microscope (SEM) image of the cross-section and corresponding energy dispersion spectrum (EDS) elemental maps.

Table 6. Chemical composition of the red box in Figure 12.

Content	O	Al	C
wt.%	50.46	47.86	1.67
at.%	62.24	35.01	2.75

The thickness variations of TGO and Al-depleted zone during the high-temperature exposure are shown in Figure 13. The standard deviation values of the TGO and Al-depleted zone thickness were calculated and listed in Table 7. It can be seen that the trends of thickness variations of TGO and the Al-depleted zone were almost the same, where the thicknesses both gradually increased from 0 to 120 h, while declining from 120 to 200 h.
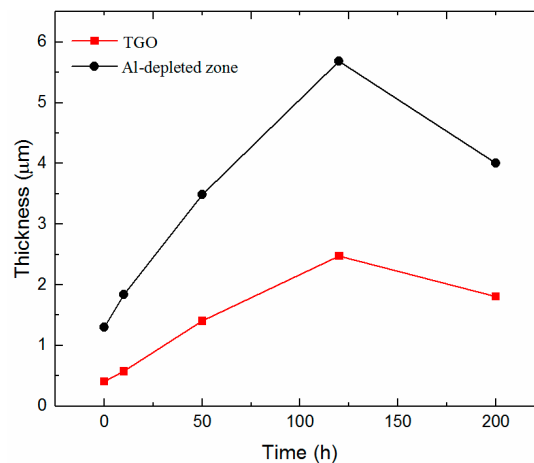

Figure 13. Variations of thickness of TGO and Al-depleted zone during the high-temperature exposure.

Table 7. The standard deviation values of TGO and Al-depleted zone thicknesses.

The Standard Deviation Values (σ)	TGO (μm)	Al-Depleted Zone (μm)
0 h	0.047	0.156
10 h	0.089	0.252
50 h	0.079	0.441
120 h	0.158	0.277
200 h	0.078	0.536

3.3. Oxidation Thermodynamics Analysis

Thermodynamic analysis can reveal whether the reaction can occur spontaneously and the stability of oxides. The oxidation reaction is determined by the standard free energy of formation in thermodynamics. The minimum thermodynamic activity of the elements that is sufficient to form the corresponding oxides can be calculated from the following Equations (2)–(4) [20].

$$\Delta G^0 = -RT \ln K_1 = -RT \ln \left[(a_{Al_2O_3}) / (a_{Al})^2 (P_{O_2})^{3/2} \right] \tag{2}$$

$$\Delta G^0 = -RT \ln K_2 = -RT \ln \left[(a_{Cr_2O_3}) / (a_{Cr})^2 (P_{O_2})^{3/2} \right] \tag{3}$$

$$\Delta G^0 = -RT \ln K_3 = -RT \ln \left[(a_{CoO}) / (a_{Co}) (P_{O_2})^{1/2} \right] \tag{4}$$

where the subscripts a refer to the thermodynamic activity of phase, and K_1, K_2, and K_3 are the equilibrium constant of Equations (2)–(4). The standard free energy of formation and equilibrium constant of oxides at 1000 °C are listed in Table 8. The corresponding oxides are formed when the oxygen pressure is larger than the minimum partial pressures of oxygen. From Table 8, it is indicated that Al needs the minimum thermodynamic activity to form Al_2O_3. Meanwhile, the minimum oxygen partial pressure of Al_2O_3 is smaller than those of Cr_2O_3 and CoO [19,21,22], which means that Al_2O_3 forms more easily than Cr_2O_3 and CoO during the high-temperature exposure.

Table 8. The Gibbs free energies and oxygen partial pressure of oxides formation at 1000 °C [20,22].

Oxides	Standard Free Energy of Formation, ΔG^0 (kJ/mol)	Equilibrium Constant, K_i	The Minimum Oxygen Partial Pressure (Pa)	Elements	Thermodynamic Activity of Elements
Al_2O_3	−1613.1	1.56×10^{66}	1.32×10^{-30}	Al	8.03×10^{-34}
Cr_2O_3	−1027	1.39×10^{42}	2.53×10^{-17}	Cr	8.47×10^{-22}
CoO	−171.7	1.1×10^7	1.62×10^{-7}	Co	3.01×10^{-4}

4. Discussions

The above results show that the oxides formed by TGO at the different stages of exposure are different. Co and Cr oxides are mainly formed at the stages of 0–10 h and after 120 h, and the Al_2O_3 is mainly formed at the stage of 10–120 h and about 200 h, and there is an interaction between the Al_2O_3 and Cr and Co oxides during the high-temperature exposure, which is the result of the major factor affecting the formation of oxides at different stages. Additionally, the thickness variations of the TGO and Al-depleted zone are related to the oxides formed. Based on the growth behavior of TGO, high-temperature exposure can be characterized by three stages.

At the initial stage of exposure (0–10 h), oxygen needs to pass through the YSZ top coat to reach the TC/BC interface, while elements such as Al, Cr and Co in the bond coat need to diffuse to the TC/BC interface to react with oxygen. As the oxides formed at this stage are insufficient to fully cover the TC/BC interface, a dense and continuous oxide scale is not formed. The oxide scale formed at this stage cannot hinder oxygen diffusing from the YSZ top coat to the TC/BC interface, thus the TBC shows a fast initial oxidation rate at the beginning of oxidation. Therefore, the formation of oxides mainly depends on the diffusion rate of Al^{3+}, Cr^{3+} and Co^{2+}. Thermodynamics do not play a dominant role at this stage. The diffusion coefficients of Al^{3+}, Cr^{3+} and Co^{2+} can be calculated by Equation (5):

$$D = D_0 e^{-\frac{Q}{RT}} \tag{5}$$

where D is the diffuse coefficient, Q represents the activation energy of diffusion, and D_0 is the frequency factor. According to Table 9, the diffusion coefficient of Co^{2+} is larger than those of Al^{3+} and Cr^{3+}, and the diffusion coefficient of Al^{3+} is smaller than that of Cr^{3+}. Therefore, Cr and Co preferentially react with oxygen before Al at the initial stage of exposure. Additionally, a small amount of oxides are formed at this stage, and thus the thicknesses of the TGO increase.

Table 9. The diffusion coefficients of Al^{3+}, Cr^{3+} and Co^{2+} at 1273 K.

Element	D_0 (m^2/s)	Q (J/mol)	D (m^2/s)
Al^{3+}	1.5×10^{-2}	4.70×10^5	7.76×10^{-22}
Cr^{3+}	0.4	4.18×10^5	2.82×10^{-18}
Co^{2+}	0.5	2.51×10^5	2.76×10^{-11}

At the second stage of exposure (10–120 h), which can also be named the steady oxidation stage, elements such as Al, Cr and Co reach the TC/BC interface. Then the reactions are determined by the thermodynamics of Al, Cr and Co. The minimum thermodynamic activity to form the corresponding oxide of Al is lower than those of Co and Cr, and the minimum oxygen partial pressure of Al is also smaller than those of Co and Cr. Therefore, large quantities of Al_2O_3 are preferentially formed at this stage, and the TGO thickness steady increases. Meanwhile, Al at the TGO/BC interface is severely consumed, and the β-CoAl phase is depleted near the TGO/BC interface, thus the thickness of the Al-depleted zone steadily increases, which is consistent with the TGO variation. Furthermore, a dense and continuous oxide scale is gradually formed, which can prevent the diffusion of oxygen, and thus the oxidation rate gradually slows down and a small amount of Cr and Co oxides are formed at the

TGO/BC interface. This result is consistent with Taylor's study [13] which demonstrates that a bond coat with asperities of high aspect ratios can result in the rapid conversion of the asperity into Co- and Cr-rich oxides.

At the last stage of exposure (120–200 h), as the severe consumption of the β-CoAl phase occurs near the TGO/BC interface, the Al content decreases. Thus there is not sufficient Al to be oxidized, and hence the formation of Al_2O_3 decreases. Then, oxygen mainly reacts with Cr and Co, causing more Cr and Co oxides to be formed near the TGO/BC interface. With Al in the deep layer of the bond coat diffusing to the TGO/BC interface, the Al content gradually increases at the TGO/BC interface, and thus the thickness of the Al-depleted zone declines. When the Al content meets the requirement for the formation of Al_2O_3, Al is oxidized again to form Al_2O_3, which surrounds the Cr and Co oxides at the TGO/BC interface. Meanwhile, a replacement reaction occurs in which Al combines with Cr_2O_3 to form Al_2O_3 [22], which leads to the densification of the oxide scale. Additionally, the phase conversion from γ-Al_2O_3 to α-Al_2O_3 causes the volume shrinkage of the oxide scale [5,23]. Therefore, both the replacement reaction of Cr_2O_3 and the phase conversion of Al_2O_3 lead to the TGO thickness declining between 120 and 200 h. The oxidation kinetics are relatively stable at this stage, and the oxidation rate follows the sub-parabolic law during the high-temperature exposure.

5. Conclusions

The high-temperature exposure test was performed at 1000 °C for 10, 50, 80, 120 and 200 h, respectively. The oxidation thermodynamics and kinetics were analyzed. The morphology and composition analysis of the TC/BC interface at different exposure time were investigated. Finally, the elemental maps of the TGO were analyzed by using EDS. The following conclusions can be drawn:

- For the whole high-temperature oxidation, the oxides were primarily Al_2O_3 and a small amount of Cr and Co oxides at the TC/BC interface. The Cr and Co oxides were mainly formed at the initial stage when the oxidation behavior mainly depended on the diffusion rate and after 120 h of exposure when Al at the TGO/BC interface was not sufficient to be oxidized.
- The high-temperature exposure can be characterized by three different stages. At the initial exposure stage (0–10 h), the formation of oxides mainly depended on the diffusion rate. Thus Cr and Co were oxidized before Al. At the steady oxidation stage (10–120 h), as the thermodynamics takes a dominant role, the main oxides were Al_2O_3. At the last stage (120–200 h), Cr and Co were oxidized with the consumption of Al at the TGO/BC interface. Both the replacement reaction of Cr_2O_3 and the phase conversion of Al_2O_3 led the TGO thickness to decline from 120 to 200 h.
- In future work, to reveal the influences of Cr and Co on TGO growth quantitatively, it is necessary to investigate the corresponding Al content in the bond coat when Cr and Co begin to be oxidized and when Al_2O_3 starts to be formed again at the last stage of exposure.

Author Contributions: H.W. and W.Z. conceived and designed the experiments; J.Z. and W.L. performed the experiments; J.Z. and W.Z. analyzed the data; X.L. contributed reagents/materials/analysis tools; J.Z. and H.W. wrote the paper.

References

1. Goward, G.W. Progress in coatings for gas turbine airfoils. *Surf. Coat. Technol.* **1998**, *108–109*, 73–79. [CrossRef]
2. Clarke, D.R.; Oechsner, M.; Padture, N.P. Thermal-barrier coatings for more efficient gas-turbine engines. *MRS Bull.* **2012**, *37*, 891–898. [CrossRef]

3. Zhu, D.; Szewciw, L.; Vernerey, F.; Barthelat, F. Puncture resistance of the scaled skin from striped bass: Collective mechanisms and inspiration for new flexible armor designs. *J. Mech. Behav. Biomed. Mater.* **2013**, *24*, 30–40. [CrossRef] [PubMed]

4. Tolpygo, V.K.; Clarke, D.R.; Murphy, K.S. Oxidation-induced failure of EB-PVD thermal barrier coatings. *Surf. Coat. Technol.* **2001**, *146–147*, 124–131. [CrossRef]

5. Shillington, E.A.G.; Clarke, D.R. Spalling failure of a thermal barrier coating associated with aluminum depletion in the bond-coat. *Acta Mater.* **1999**, *47*, 1297–1305. [CrossRef]

6. Ji, Q.; Song, P.; Wang, Y.; Liao, H.; Liu, J. Effect of Co and Ni contents in MCrAlY bondcoats on microstructure and lifetime of APS TBC systems. *J. Funct. Mater.* **2016**, *47*, 74–78. (In Chinese) [CrossRef]

7. Ansari, M.; Shoja-Razavi, R.; Barekat, M.; Man, H.C. High-temperature oxidation behavior of laser-aided additively manufactured NiCrAlY coating. *Corros. Sci.* **2017**, *118*, 168–177. [CrossRef]

8. Liang, T.; Guo, H.; Peng, H.; Gong, S. Microstructural evolution of CoCrAlY bond coat on Ni-based superalloy DZ 125 at 1050 °C. *Surf. Coat. Technol.* **2011**, *205*, 4374–4379. [CrossRef]

9. Gao, J.; He, Y.; Wang, D. Preparation of YSZ/Al_2O_3 micro-laminated coatings and their influence on the oxidation and spallation resistance of MCrAlY alloys. *J. Eur. Ceram. Soc.* **2011**, *31*, 79–84. [CrossRef]

10. Keyvani, A. Microstructural stability oxidation and hot corrosion resistance of nanostructured Al_2O_3/YSZ composite compared to conventional YSZ TBC coatings. *J. Alloys Compd.* **2015**, *623*, 229–237. [CrossRef]

11. Chen, W.R.; Wu, X.; Marple, B.R.; Nagy, D.R.; Patnaik, P.C. TGO growth behaviour in TBCs with APS and HVOF bond coats. *Surf. Coat. Technol.* **2008**, *202*, 2677–2683. [CrossRef]

12. Allen, A.T.; Douglass, D.L. Internal carburizing behavior of Ni-V, Ni-Cr, and Ni-3Nb alloys. *Oxid. Met.* **1999**, *52*, 505–536. [CrossRef]

13. Taylor, M.P.; Pragnell, W.M.; Evans, H.E. The influence of bond coat surface roughness on chemical failure and delamination in TBC systems. *Mater. Corros.* **2008**, *59*, 508–513. [CrossRef]

14. Chen, W.R.; Archer, R.; Huang, X.; Marple, B.R. TGO growth and crack propagation in a thermal barrier coating. *J. Therm. Spray Technol.* **2008**, *17*, 858–864. [CrossRef]

15. Bansal, N.P.; Zhu, D. Effects of doping on thermal conductivity of pyrochlore oxides for advanced thermal barrier coatings. *Mater. Sci. Eng. A* **2007**, *459*, 192–195. [CrossRef]

16. Zhu, D.; Choi, S.R.; Miller, R.A. Thermal fatigue and fracture behavior of ceramic thermal barrier coatings. In *25th Annual Conference on Composites, Advanced Ceramics, Materials, and Structures: B: Ceramic Engineering and Science Proceedings*; Singh, M., Jessen, T., Eds.; John Wiley & Sons, Inc.: Hoboken, NJ, USA, 2001; Volume 22, pp. 453–461.

17. Liang, T.; Guo, H.; Peng, H.; Gong, S. Precipitation phases in the nickel-based superalloy DZ 125 with YSZ/CoCrAlY thermal barrier coating. *J. Alloys Compd.* **2011**, *509*, 8542–8548. [CrossRef]

18. Walter, M.E.; Eigenmann, B. The mechanical response of three EB-PVD thermal barrier coating microstructures. *Mater. Sci. Eng. A* **2000**, *282*, 49–58. [CrossRef]

19. Tang, F.; Ajdelsztajn, L.; Schoenung, J.M. Influence of cryomilling on the morphology and composition of the oxide scales formed on HVOF CoNiCrAlY coatings. *Oxid. Met.* **2004**, *61*, 219–238. [CrossRef]

20. Nath, S.; Manna, I.; Majumdar, J.D. Kinetics and mechanism of isothermal oxidation of compositionally graded yttria stabilized zirconia (YSZ) based thermal barrier coating. *Corros. Sci.* **2014**, *88*, 10–22. [CrossRef]

21. Li, T.; Li, Y.; Li, J.; Li, W.; Liu, G.; Mi, Z.; Wang, L.; Lv, P. Oxidation behavior of high-velocity oxygen fuel sprayed MCrAlY coatings. *Proc. Chin. Soc. Electr. Eng.* **2014**, *34*, 176–181.

22. Yamano, H.; Tani, K.; Harada, Y.; Teratani, T. Oxidation control with chromate pretreatment of MCrAlY unmelted particle and bond coat in thermal barrier systems. *J. Therm. Spray Technol.* **2008**, *17*, 275–283. [CrossRef]

23. Chen, H.; Li, Q.; Cheng, X.; Chen, L. Influence of thermally grown oxide on failure of thermal barrier coating. *Mater. Prot.* **2012**, *45*, 5–7. (In Chinese)